Progress In Electromagnetics Research M, Vol. 85, 135–144, 2019

Detection of Water Content in Emulsified Oil with the Metamaterial Sensor

Jie Huang*, Zhi-Hua Wei, Guo-Qing Xu, Jun-Shan Li, and Jing Li

Abstract—A metamaterial sensor that can be applied to detect water content in emulsified oil is proposed, which is reusable in experiment and nondestructive to the sample. Electric field of the original absorber is researched to guide the design of microfluidics. Also, its equivalent circuit model is proposed to validate its ability as a sensor. The calculated sensitivity of the sensor is 339 MHz/ε'_r in the range of 11.26 GHz to 10.044 GHz, indicating its potential for detecting the emulsified oil. The experimental results reveal the reliable process of detection and the linear relationship between frequency shift and water content. This work provides a fast and convenient solution to check the quality of lubricant oil to some extent, which is relatively valuable to modern machinery.

1. INTRODUCTION

With industrial revolution, booming machinery undoubtedly gives rise to the wide application of lubricant oil. Due to complex working environment, lubricant oil can be contaminated and emulsified by water. Even small amount of water can accelerate the oil oxidation and reduce its performance [1, 2]. This can damage the machine, such as triggering the consequence of micro-pitting on gears [3]. Traditional methods of checking the quality of lubricant oil are based on evaporation and distillation which are precise but tedious [4]. Although the surface acoustic wave devices [5] simplify the operation to some extent the operation of evaporation is inevitable, and the content of sample is relatively larger. After that, the method of infrared spectroscopes [6] is proposed to quickly detect the oil, but the larger water droplets in oil may produce more variabilities in detection. It limits the further development of oil measurement, and a fast method with the properties of micro sampling is valuable. Given that substance can be characterized by permittivity, the technique based on metamaterial absorber will be a potential candidate for detection.

The metamaterial absorber owning near perfect properties of absorption [7–11] is popular with the researchers. Most of the works have been done towards developing multi-band and broadband absorbers, which can be applied in the areas of imaging [12], stealthy material [13], and energy harvesting [14, 15]. Nowadays, a new branch of absorber, functioning as sensor, begins to burgeon by utilizing the characteristic of being sensitive to the permittivity. With a reasonable configuration, it can detect sucrose [16], strain [17], temperature [18], permittivity of solid [19, 20], and liquid [21–24]. For the detection of liquid, conventional sensor based on metamaterial absorber may produce more errors in the situation that fluid is relatively harder to be limited on certain extent of resonance region, resulting in higher requirement of operation in experiment [25]. However, the method of loading microfluidic [26, 27] enhances the feasibility of operating with fluid medium, promoting a wider range of liquids [28, 29] to be detected.

In this paper, a compact sensor based on a metamaterial absorber is proposed to detect the water content of emulsified oil. An original absorber is firstly designed to act as a fundamental structure, and

Received 30 June 2019, Accepted 13 September 2019, Scheduled 24 September 2019
* Corresponding author: Jie Huang (jiehuang@swu.edu.cn).
The authors are with the College of Engineering and Technology, Southwest University, Chongqing 400715, China.

the equivalent circuit model of the resonator simulated by ADS software further suggests its potential for sensing. Through the analysis of the mechanism, strong resonance region is found to guide the design of the microfluidic. The sensor shows that it can achieve the sensitivity of 339 MHz/ε'_r (ε'_r is the real part of dielectric constant). To prove the rationality of design, the sensor is fabricated to detect the water content in emulsified oil. Experimental result is highly consistent with the simulated one and shows a good linear trend, indicating the potential value of the proposed absorber for sensing applications.

2. DESIGN OF SENSOR

The original metamaterial absorber, consisting of a resonator and a film that are divided by the dielectric layer (substrate), is displayed in Fig. 1. Its simulated structure parameters are presented in follows: $W_1 = 0.15\,\text{mm}$, $W_2 = 0.1\,\text{mm}$, $S = 10.16\,\text{mm}$, $L = 20.86\,\text{mm}$, $R_0 = 2.05\,\text{mm}$, $\theta = 14°$, $\alpha = 8°$, $t_1 = 0.035\,\text{mm}$, $t_2 = 1\,\text{mm}$. The pattern and film are fabricated by copper with the conductivity of $\sigma = 5.8 \times 10^7\,\text{S/m}$, while the dielectric layer is low loss material named Rogers RO4003 whose dielectric constant is $\varepsilon = 3.55\ (1 + i0.0027)$.

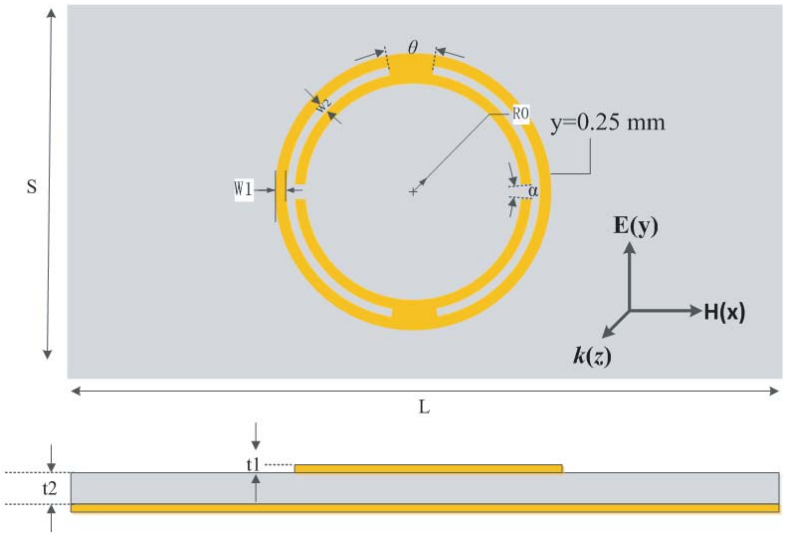

Figure 1. Diagram of original absorber, including the front view and lateral view.

All the simulated results are achieved by the finite integration technique, where a plane electromagnetic (EM) wave with the electric field pointing to the y-axis is applied as the exciting source. In addition, an open (add space) condition is set along the z-axis, while conducting wall conduction is applied in the direction of x-axis and y-axis. Due to the situation that the thickness of bottom metallic film is larger than skin depth, transmission T_ω is approximated to 0, and the absorption A_ω can be calculated by the expression $A_\omega = 1 - R_\omega$, where R_ω is the reflection. The spectrum of absorption is presented in Fig. 2. It shows a single peak at 9.9 GHz with the absorption rate over 99%, which can be considered as the index of sensor.

Figure 3 presents the distributions of electrical field ($|E|$). From the electrical field on the interface of resonator and dielectric layer, strong resonance region mainly concentrates around the middle split and inner ring of the resonator, which can guide the layout of microchannel. From the cross section of $|E|$ at $y = 0.25\,\text{mm}$ (see in the Fig. 1), the intensity of electrical field decreases with the increase of distance from the resonator pattern. It suggests that the layer of microchannel should be closer to the resonator, so as to generate a stronger interaction between the electrical field and material under test, and finally improve the sensitivity.

To validate the ability of the absorber as a sensor, the relationship between absorption frequency and dielectric constant is researched by constructing a simplified equivalent circuit [30] of resonator. The gap of resonator can be treated as capacitor, while the metallic part in resonator can be regarded

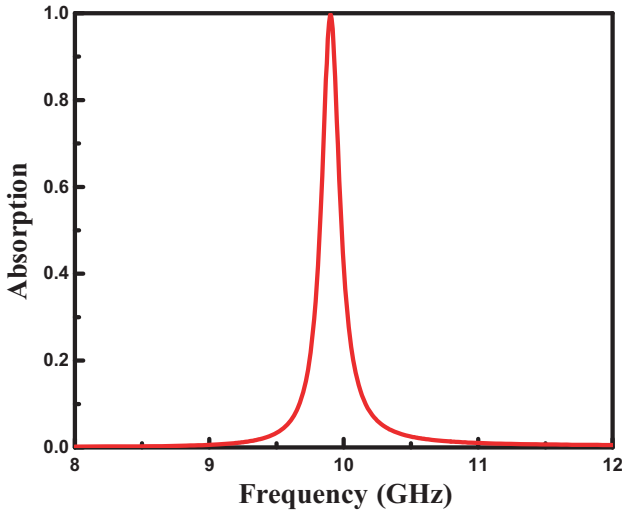

Figure 2. The spectrum of absorption for the original absorber.

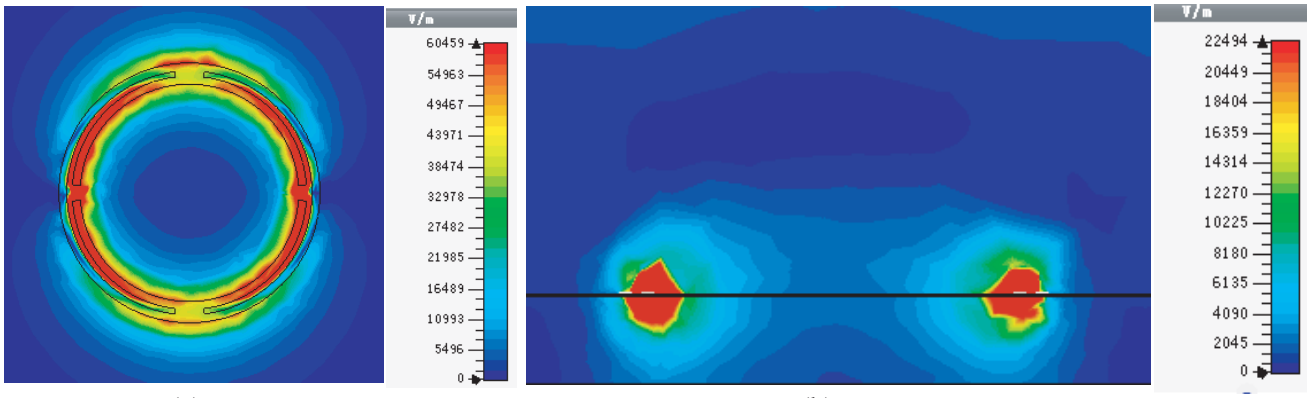

(a) (b)

Figure 3. (a) Electric field of original absorber at the interface of resonator and dielectric layer. (b) Electric field in the cross section of $y = 0.25$ mm.

as inductor, and the corresponding capacitance and inductance can be obtained by the lumped element extraction method of distributed component [31]. Ignoring the influence of impedance, the diagram of equivalent circuit is presented in Fig. 4, and the expression of impedance is given as:

$$Z=\frac{L_2\omega(2C_1L_1\omega^2j+C_2L_1\omega^2j-j)}{2C_1L_1\omega^2+2C_1L_2\omega^2++C_2L_1\omega^2+C_2L_2\omega^2-1} \tag{1}$$

Set $Z = 0$ in Equation (1), and the formula of frequency can be obtained as:

$$2C_1L_1\omega^2+C_2L_1\omega^2-1=0 \tag{2}$$

$$f=\frac{1}{2\pi}\sqrt{\frac{1}{2C_1L_1+C_2L_1}} \tag{3}$$

Based on Eq. (3), Fig. 5 presents the computed results of equivalent circuit after extracting parameter in the soft Advanced Design System (ADS), which is relatively consistent with the results in the CST. As the dielectric constant of substrate increases, the resonance frequency gradually decreases, suggesting the detection principle that dielectric constant of material can be characterized by frequency shift.

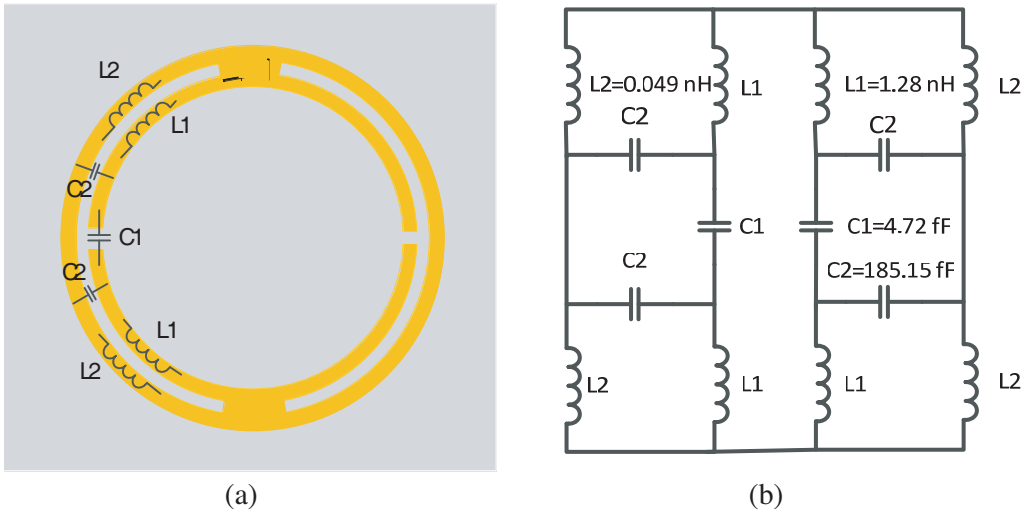

Figure 4. (a) Equivalent diagram of capacitance and inductance. (b) Equivalent circuit diagram.

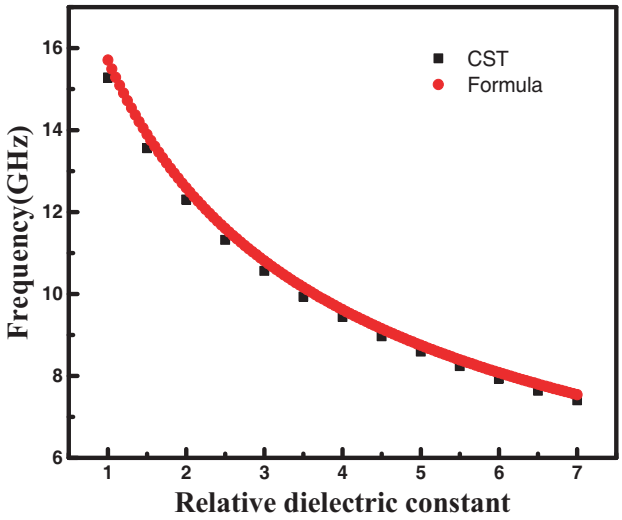

Figure 5. The relationship between frequency point and dielectric constant. The black scatter point is simulated by the soft of CST and the red curve is calculated by formula.

Microfluidics is loaded on the middle layer after dividing the original absorber into two parts, as shown in Fig. 6(a). According to the distribution of electrical field above, the position of microchannel should be near the resonator, whereas limited by the fabrication technique, the thickness of Rogers RO4003 can only be reduced to 0.254 mm. The material of microfluidics is polytetrafluoroethylene (PTFE), which can prevent the sensor from corrosion and adhesion by emulsified oil. As presented in Fig. 6(b), the structure parameters of microfluidics are shown as follows: $P = 1.47$ mm, $a = 0.43$ mm, $R_1 = 1.277$ mm, $R_2 = 2.83$ mm, $R_3 = 4.73$ mm, $t_3 = 0.4$ mm, $t_4 = 0.4$ mm. The measured liquid can be injected from port 1 to port 2. Fig. 6(a) only shows the resonance part of the sensor, which is loaded in the waveguide and directly irradiated by the EM wave. To add the injecting pedestal and fit the dimension of waveguide, the length of sensor is properly prolonged. Photos of the integral sensor are shown in Figs. 6(c) and (d), and three layers are adhered by insulating glue.

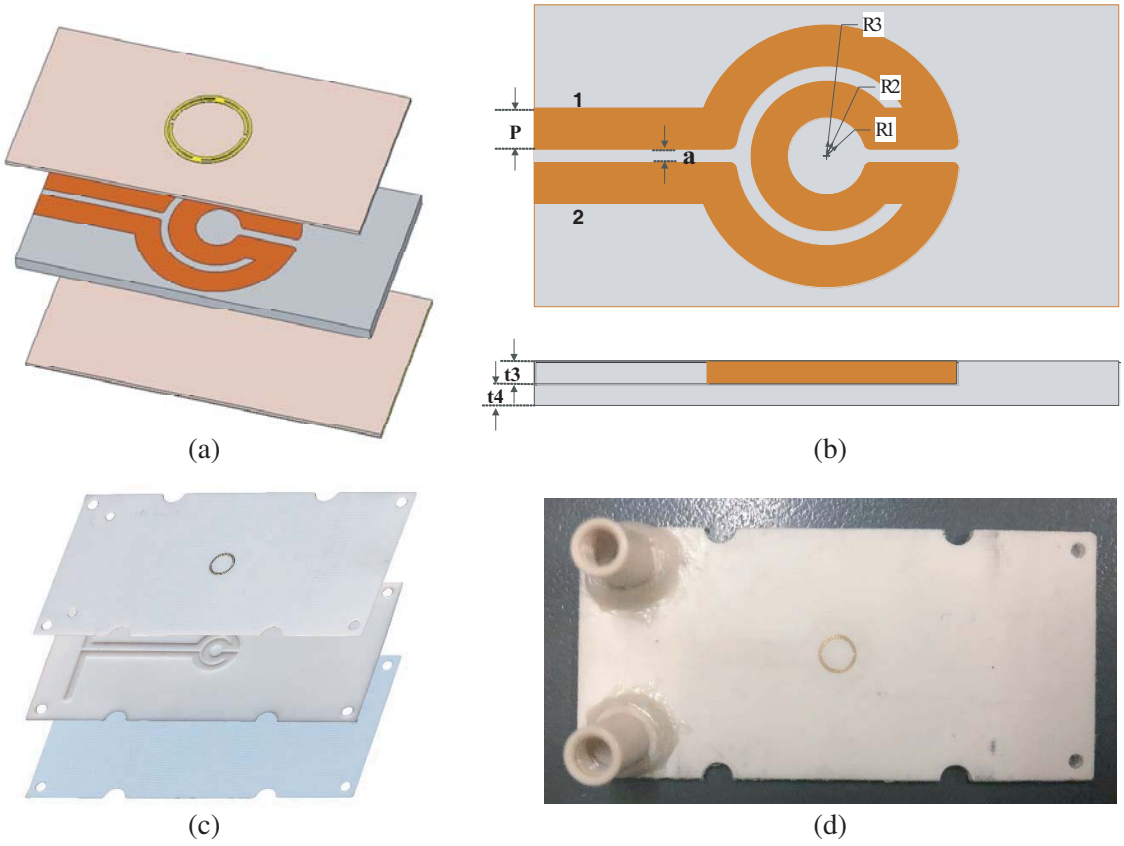

Figure 6. (a) Schematic diagram of microfluidic. (b) Spatial stereogram of the sensor. (c) Three layers of the fabricated sensor. (d) Fabricated sensor.

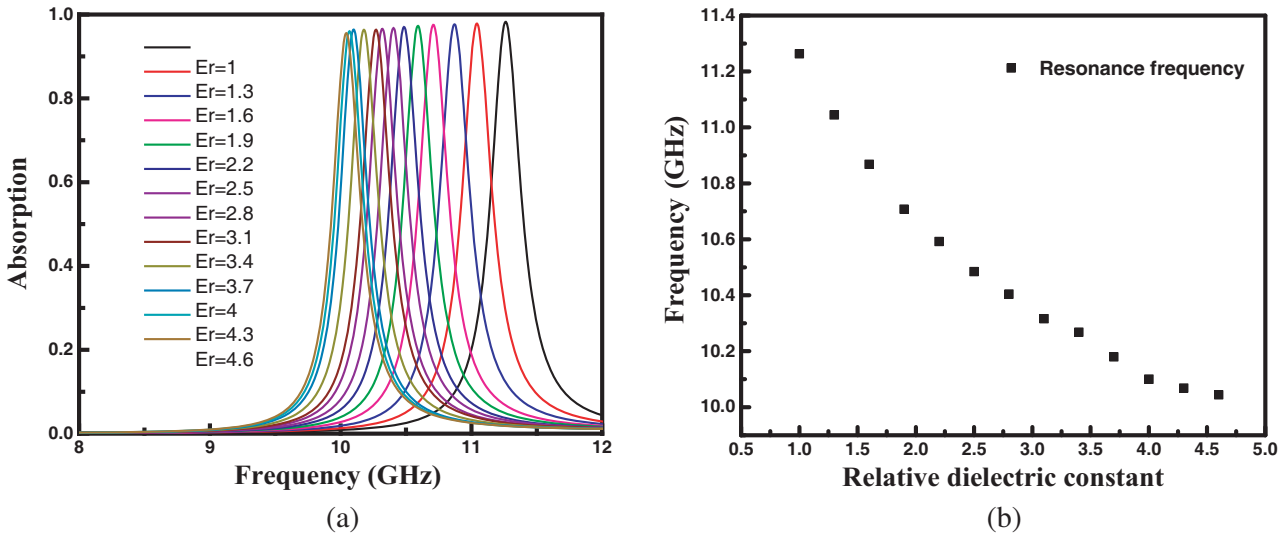

Figure 7. (a) Spectrum of the absorption peak of the sensor varying with dielectric constant. (b) Scatter plot of the dielectric constant corresponding to the frequency.

3. RESULTS AND DISCUSSION

The simulated results of sensor are depicted in Fig. 7. As the dielectric constant increases from 1 to 4.6, the frequency has a red shift from 11.26 GHz to 10.044 GHz, reaching the sensitivity of 339 MHz/ε'_r. These results illustrate that the sensor proposed here can effectively detect the liquid whose dielectric constant is in the range from 1 to 4.6. Fig. 8 presents the electrical field of the sensor on two different cross sections. Although its strength is less than that of original absorber because of changing the optimal resonance mode, the strong resonance region concentrates around the microfluidics, ensuring the capacity of detection. Also, the sensitivity of sensor is relatively low compared with that of original absorber shown in Fig. 5. This is because the effective volume for dielectric constant variation area has decreased (i.e., from the whole substrate to only microchannel area).

Figure 9 exhibits the connection diagram in test, where the emulsified oil is injected into the sensor by the syringe pump. Due to the metallic film, transmission coefficient S_{21} is approximated to 0. Vector network analyzer only needs to be connected with one port of the standard WR-90 waveguide (dimension: 2.286 cm $\times$ 1.016 cm) to record the reflection coefficient S_{11} whose resonance peak is at 10.404 GHz when the microchannel is filled with air. Emulsified oil with different water contents from

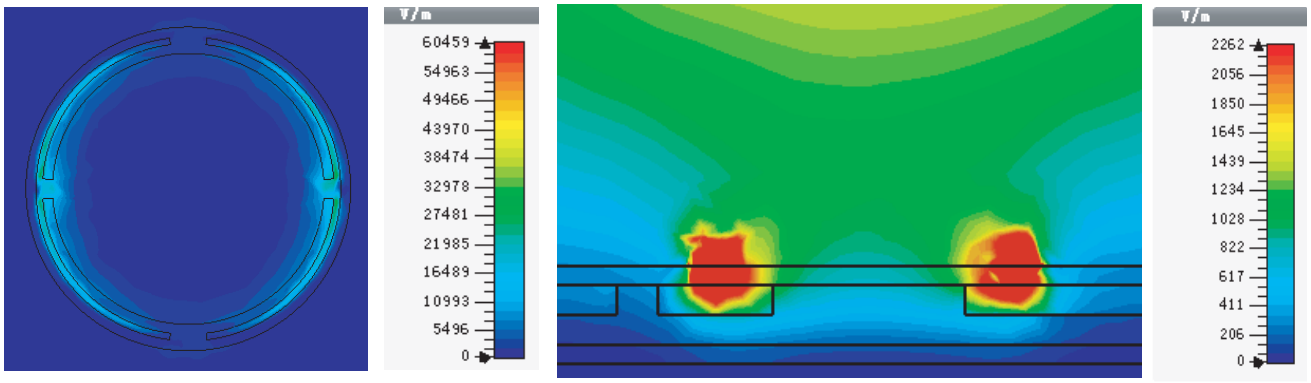

(a) (b)

Figure 8. (a) Electric field distribution of sensor at the interface of resonator and dielectric layer. (b) Distribution of electric field in the cross section of $y = 0.25$ mm.

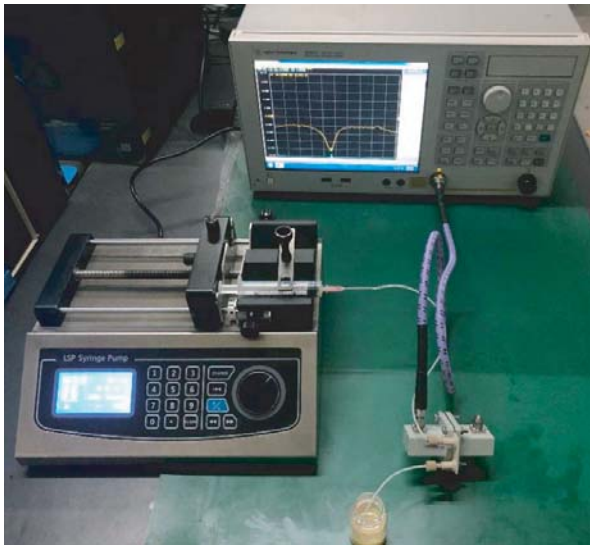

Figure 9. Connection diagram in test.

1% to 9% is repeatedly tested four times. With the increase of water content, the average resonance frequency linearly decreases from 10.171 GHz to 10.100 GHz, which can be seen in Fig. 10. Error bars show that the maximum error among the four tests for the same water content is no more than 8 MHz, indicating a stable performance in detection. The relationship between average frequency and water content is $y1 = -0.00863x + 10.177$ after linearly fitting with correction coefficient of 0.9936. According to the resonance frequency of microchannel filled with air, the average frequency shift of different water contents in emulsified oil is also depicted in Fig. 10. Its relationship between frequency shift and water content is $y2 = 8.65x + 226.55$ with correction coefficient of 0.9938. Thus, the calculating formula of water content in emulsified oil is $x = (y2 - 226.55)/8.65$.

It is noticed that there are obvious deviations of frequency between the simulation and experiment when the microchannel is filled with air (at the frequency of 11.26 GHz in simulation and 10.404 GHz in

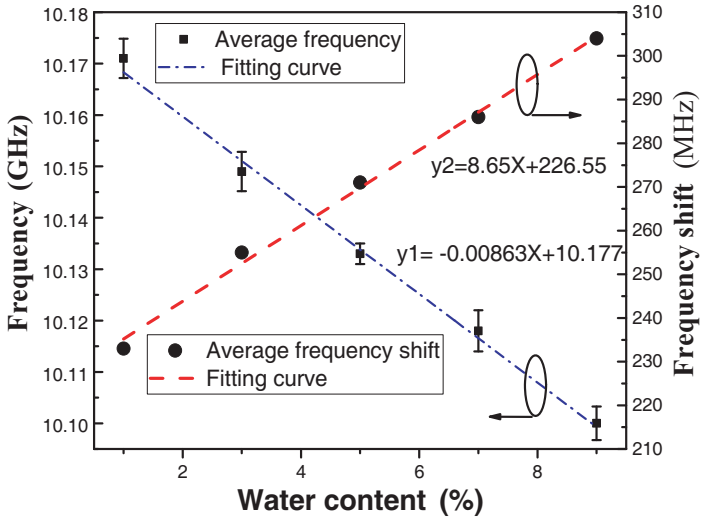

Figure 10. Scatter plot for mean resonance frequency and offset, and fitting them linearly.

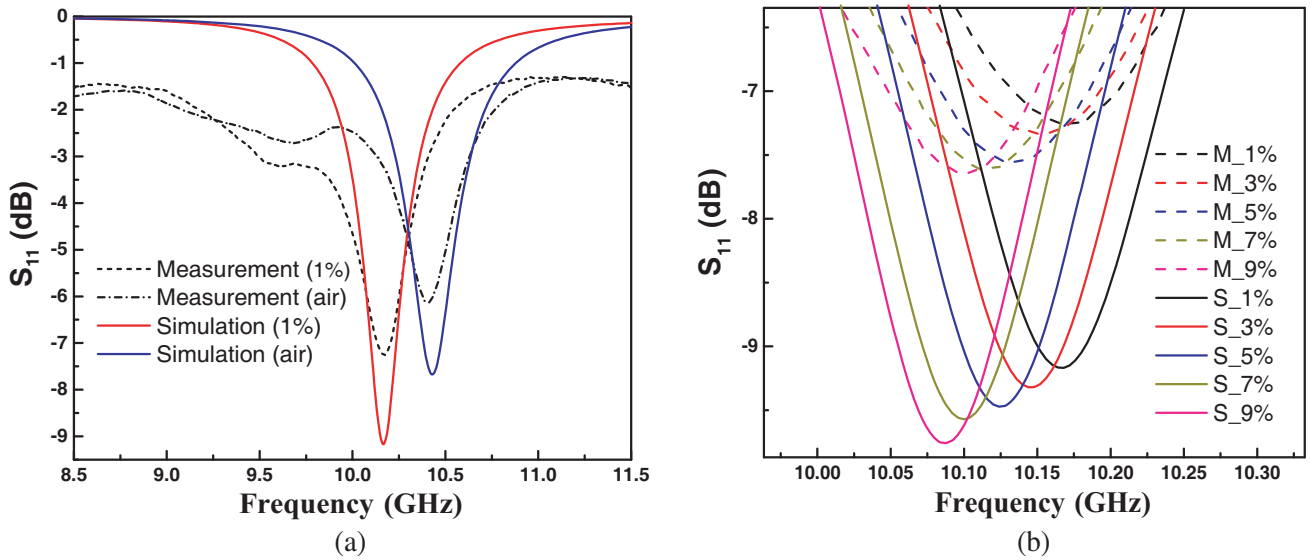

Figure 11. (a) Empty (air) and 1% water content for measurement and simulation chart. (b) Spectrum of simulation and measurement under different water content, where dashed line is measured and solid line is simulated.

experiment). These frequency deviations should come from fabrication tolerances. In order to decrease the disparity between simulated and measured results, actual geometrical parameters of the fabricated sensor prototype are measured using a microscope, and then the simulated results are calibrated by using these actually measured geometrical parameters in simulations. Fig. 11 shows the after-calibrated simulation and experiment results when the sensor is empty and contains the emulsified oil with 1% to 9% water content. In order to obtain the corresponding simulated S_{11} of the sensor, the permittivities of pure water of $63 - 30i$ and pure emulsified oil of $1.82 - 0.269i$ are measured first by using Keysight coaxial probe kit (N1500A), respectively. Then, permittivities of the emulsified oil with 1% to 9% water content are calculated by using the following dielectric mixture Equation (4) [27]:

$$\varepsilon_m = \varepsilon_{eo} \cdot \left[\frac{(2\varepsilon_{eo} + \varepsilon_w) + 2V_f (\varepsilon_w - \varepsilon_{eo})}{(2\varepsilon_{eo} + \varepsilon_w) - V_f (\varepsilon_w - \varepsilon_{eo})} \right] \tag{4}$$

where ε_m, ε_{eo}, and ε_w represent permittivities of the emulsified oil-water mixture, pure emulsified oil, and pure water, respectively. V_f is the volume fraction of water in the emulsified oil-water mixtures. These calculated effective permittivities of the 1%, 3%, 5 %, 7%, and 9% moisture emulsified oils are 1.8710, 1.9758, 2.0846, 2.1978, and 2.3156, respectively. They are input to electromagnetic simulator CST to obtain the simulated reflection coefficient S_{11} of the sensor under different water contents. They have highly consistent trends that the frequency has red shifts with the increase of water content, showing the validity in the process of design.

4. CONCLUSION

A microfluidic-based metamaterial sensor is proposed which shows stable and high characteristics in detecting a small amount of emulsified oil. The electric field of an original absorber is researched to guide the design of microfluidic, and its equivalent circuit is constructed to further verify its ability as a sensor. The sensor shows a high sensing capability ($339\,\mathrm{MHz}/\varepsilon'_r$) in the range of 11.26 GHz to 10.044 GHz, which is adequate to detect emulsified oil with different water contents. The experiment is repeatedly operated, and a linear expression about the frequency shift and water content is obtained. This sensor overcomes time-consuming drawbacks and shows a reusable and nondestructive solution to recognize the quality of lubricant oil and enhance the life of machinery.

ACKNOWLEDGMENT

This work was supported in part by the National Natural Science Foundation of China (Grant No. 61401373 and No. 61971358), in part by the Fundamental Research Funds for the Central Universities (Grant No. XDJK2018B017 Grant No. XDJK2019D016), and in part by the Research Fund for the Doctoral Program of Southwest University (Grant No. SWU111030).

REFERENCES

1. Pourya, P., A. Ghanbarzadeh, M. Wilson, et al., "An experimental and analytical study of the effect of water and its tribochemistry on the tribocorrosive wear of boundary lubricated systems with ZDDP-containing oil," *Wear*, Vol. 358–359, No. 15, 23–31, 2016.
2. Harika, E., J. Bouyer, M. Fillon, et al., "Effects of water contamination of lubricants on hydrodynamic lubrication: Rheological and thermal modeling," *Journal of Tribology — Transactions of the ASME*, Vol. 135, No. 4, 041707, 2013.
3. Engelhardt, C., J. Witzig, T. Tobie, et al., "Influence of water contamination in gear lubricants on wear and micro-pitting performance of case carburized gears," *Industrial Lubrication and Tribology*, Vol. 69, No. 4, 612–619, 2017.
4. Larsson, W., J. Jalbert, R. Gilbert, et al., "Efficiency of methods for Karl Fischer determination of water in oils based on oven evaporation and azeotropic distillation," *Analytical Chemistry*, Vol. 75, No. 6, 1227–1232, 2003.

5. Mao, Z. B., J. X. Zhao, W. P. Xuan, et al., "Distilling determination of water content in hydraulic oil with a ZnO/glass surface acoustic wave device," *Microsystem Technologies*, Vol. 23, No. 6, 1841–1845, 2017.
6. Holland, T., A. M. Abdul-Munaim, D. G. Watson, et al., "Importance of emulsification in calibrating infrared spectroscopes for analyzing water contamination in used or in-service engine oil," *Lubricants*, Vol. 6, No. 2, 35, 2018.
7. Landy, N. I., S. Sajuyigbe, J. J. Mock, et al., "Perfect metamaterial absorber," *Physical Review Letters*, Vol. 100, No. 20, 207402, 2008.
8. Hu, C. G., Z. Y. Zhao, X. N. Chen, et al., "Realizing near-perfect absorption at visible frequencies," *Optics Express*, Vol. 17, No. 13, 11039–11044, 2011.
9. Wen, Q. Y., H. W. Zhang, Y. S. Xie, et al., "Dual band terahertz metamaterial absorber: Design, fabrication, and characterization," *Applied Physics Letters*, Vol. 95, No. 24, 1111, 2009.
10. Gu, C., S. B. Qu, Z. B. Pei, et al., "A metamaterial absorber with direction-selective and polarisation-insensitive properties," *Chinese Physics B*, Vol. 20, No. 3, 433–437, 2011.
11. Agarwal, S. and Y. K. Prajapati, "Broadband and polarization-insensitive helix metamaterial absorber using graphene for terahertz region," *Applied Physics A*, Vol. 122, No. 6, 561, 2016.
12. Dincer, F., O. Akgol, M. Karaaslan, E. Unal, and C. Sabah, "Polarization angle independent perfect metamaterial absorbers for solar cell applications in the microwave, infrared, and visible regime," *Progress In Electromagnetics Research*, Vol. 144, 93–101, 2014.
13. Mohammad, R. S., A. S Ramezanali, G. Hadi, et al., "Design and fabrication of a metamaterial absorber in the microwave range," *Microwave and Optical Technology Letters*, Vol. 56, No. 8, 1748–1752, 2014.
14. Akgol, O., M. Bagmanci, M. Karaaslan, et al., "Broad band MA-based on three-type resonator having resistor for microwave energy harvesting," *Journal of Microwave Power and Electromagnetic Energy*, Vol. 51, No. 2, 134–149, 2017.
15. Alkurt, F. O., O. Altintas, M. Bakir, et al., "Octagonal shaped metamaterial absorber based energy harvester," *Materials Science*, Vol. 24, No. 3, 253–259, 2018.
16. Agarwal, S. and Y. K. Prajapati, "Multifunctional metamaterial surface for absorbing and sensing applications," *Optics Communications*, Vol. 439, 304–307, 2019.
17. Jeong, H. J. and L. Sungjoon, "A stretchable radio-frequency strain sensor using screen printing technology," *Sensors*, Vol. 16, No. 11, 1839, 2016.
18. Bakir, M., M. Karaaslan, F. Dincer, et al., "Perfect metamaterial absorber-based energy harvesting and sensor applications in the industrial, scientific, and medical band," *Optical Engineering*, Vol. 54, No. 9, 097102, 2015.
19. Tang, J. Y., Z. Y. Xiao, and K. K. Xu, "Broadband ultrathin absorber and sensing application based on hybrid materials in infrared region," *Plasmonics*, Vol. 12, No. 4, 91–98, 2016.
20. Ozturk, M., U. K. Sevim, O. Akgol, et al., "An electromagnetic non-destructive approach to determine dispersion and orientation of fiber reinforced concretes," *Measurement*, Vol. 138, 356–367, 2019.
21. Abdulkarim, Y. I., L. W. Deng, O. Altıntaş, et al., "Metamaterial absorber sensor design by incorporating swastika shaped resonator to determination of the liquid chemicals depending on electrical characteristics," *Physica E: Low-dimensional Systems and Nanostructures*, Vol. 114, 113593, 2019.
22. Altintas, O., M. Aksoy, E. Unal, et al., "Artificial neural network approach for locomotive maintenance by monitoring dielectric properties of engine lubricant," *Measurement*, Vol. 145, 678–686, 2019.
23. Altintas, O., M. Aksoy, and E. Unal, et al., "Chemical liquid and transformer oil condition sensor based on metamaterial-inspired labyrinth resonator," *Journal of the Electrochemical Society*, Vol. 166, No. 6, B482–B488, 2019.
24. Tumkaya, M. A., F. Dincer, M. Karaaslan, et al., "Sensitive metamaterial sensor for distinction of authentic and inauthentic fuel samples," *Journal of Electronic Materials*, Vol. 46, No. 8, 4955–4962,

2017.

25. Liu, J. J., L. L. Fan, J. F. Ku, et al., "Absorber: A novel terahertz sensor in the application of substance identification," *Optical and Quantum Electronics*, Vol. 48, No. 2, 80, 2016.
26. Ling, K., M. Yoo, W. J. Su, et al., "Microfluidic tunable inkjet-printed metamaterial absorber on paper," *Optics Express*, Vol. 23, No. 1, 110–120, 2015.
27. Wei, Z. H., J. Huang, J. Li, et al., "A high-sensitivity microfluidic sensor based on a substrate integrated waveguide re-entrant cavity for complex permittivity measurement of liquids," *Sensors*, Vol. 18, No. 11, 4005, 2018.
28. Robiatun, R. A., F. J. Tovar-Lopez, T. Baum, et al., "Meta-atom microfluidic sensor for measurement of dielectric properties of liquids," *Journal of Applied Physics*, Vol. 121, No. 9, 094506, 2017.
29. Yoo, M., H. K. Kim, and S. Lim, "Electromagnetic-based ethanol chemical sensor using metamaterial absorber," *Sensors and Actuators B: Chemical*, Vol. 222, 173–180, 2016.
30. Alici, K. B. and E. A. Ozbay, "A planar metamaterial: Polarization independent fishnet structure," *Photonics and Nanostructures — Fundamentals and Applications*, Vol. 6, No. 1, 102–107, 2008.
31. Xie, C. F. and K. Q. Rao, *Electromagnetic Field and Electromagnetic Wave*, 3rd edition, Higher Education Press, Beijing, China, 1999.